**Copolymerization of Biomass-Derived Carboxylic Acids for Biobased Acrylic Emulsions**

Ashish Bohre,[*a] Mohammad Asif Ali,[b], Martin Ocepek,[c] Miha Grilc[a], Jožefa Zabret,[c] and Blaž Likozar[*a]

[a]*Department of Catalysis and Chemical Reaction Engineering, National Institute of Chemistry, Hajdrihova 19, 1000 Ljubljana, Slovenia*

[b]*Soft Matter Sciences and Engineering Laboratory, ESPCI Paris, PSL University, CNRS, 10 rue Vauquelin, 75005 Paris, France.*

[c]*Helios TBLUS d.o.o., Količevo 65, 1230 Domžale, Slovenia*

# Supporting Information

## 1. Experimental details

### 1.1. Materials

Itaconic acid (Sigma-Aldrich, 99%), Citric acid (Sigma-Aldrich, 99%), methacrylic acid (Sigma-Aldrich, 99%),, mesaconic acid (Sigma-Aldrich, 98%), crotonic acid (Sigma-Aldrich, 99%),, citraconic acid (Sigma-Aldrich, 99%), 2-hydroxy isobutaric acid (Sigma-Aldrich, ≥99%), Amberlyst-15 (Sigma-Aldrich), pyruvic acid, (Fluka, ≥99.5%), acetic acid (Sigma-Aldrich, 99%), acetone (Sigma-Aldrich, 99%) and palladium(II) nitrate hydrate (Fluka, 99%), Pd/C, Pt/C, Ru/C, Pd/$SiO_2$, Pd/$BaSO_4$ and Pd/$Al_2O_3$ (5 wt%, Sigma Aldrich), Aluminum nitrate nonahydrate (Sigma Aldrich, ≥ 98%), barium nitrate (Sigma-Aldrich, 99%), ammonium carbonate (Alfa Aesar), hydrochloric acid (Alfa Aesar), carbon black (Alfa Aesar), $MgAl_2O_4$ (Sigma Aldrich), $ZrO_2$ (Alfa Aesar), ZSM5-30, BEA-300, HY-30, HY-80 were purchased from commercial source.

## 2. Catalyst characterisation

### 2.1. Powder X-ray diffraction (PXRD)

The PXRD pattern of $BaAl_{12}O_{19}$ catalyst showed diffraction peaks at 21.6°, 26.9°, 31,9° 35.5°, 42.0°, 57.4°, and 66.7° similar to that of the single-phase structure of hexagonal type compound $BaAl_{12}O_{19}$ (JCPDS 00-026-0135, Fig. S1a). After loading the palladium, $BaAl_{12}O_{19}$ catalyst maintain most of their crystallinity. We have not observed the peaks correspond to palladium, signifying that PdO phases are highly dispersed (Fig. S1b).[1, 2] For all the aluminate catalysts, amorphous alumina phase is observed. The high crystalline peaks in the calcium, sodium and magnesium were corresponds to their respective oxides in addition to the mixed metal alumina phases (JCPDS No. 00-04-0880). The XRD pattern of $MgAl_2O_4$ low crystallinity compared to other hexa-aluminate due to the presence of amorphous phases of MgO and alumina (Fig. S1e). In case of CaMgO catalyst, crystalline phases of CaO (32.49°, 37.54°, 43.22°, 54.13° and 67.57°), MgO (62.52°, 64.47°, 74.95° and 78.86°) and $CaCO_3$ (23.15°, 29.54°, 39.68°, 47.31° and 48.76°) were observed (Fig. S1f).

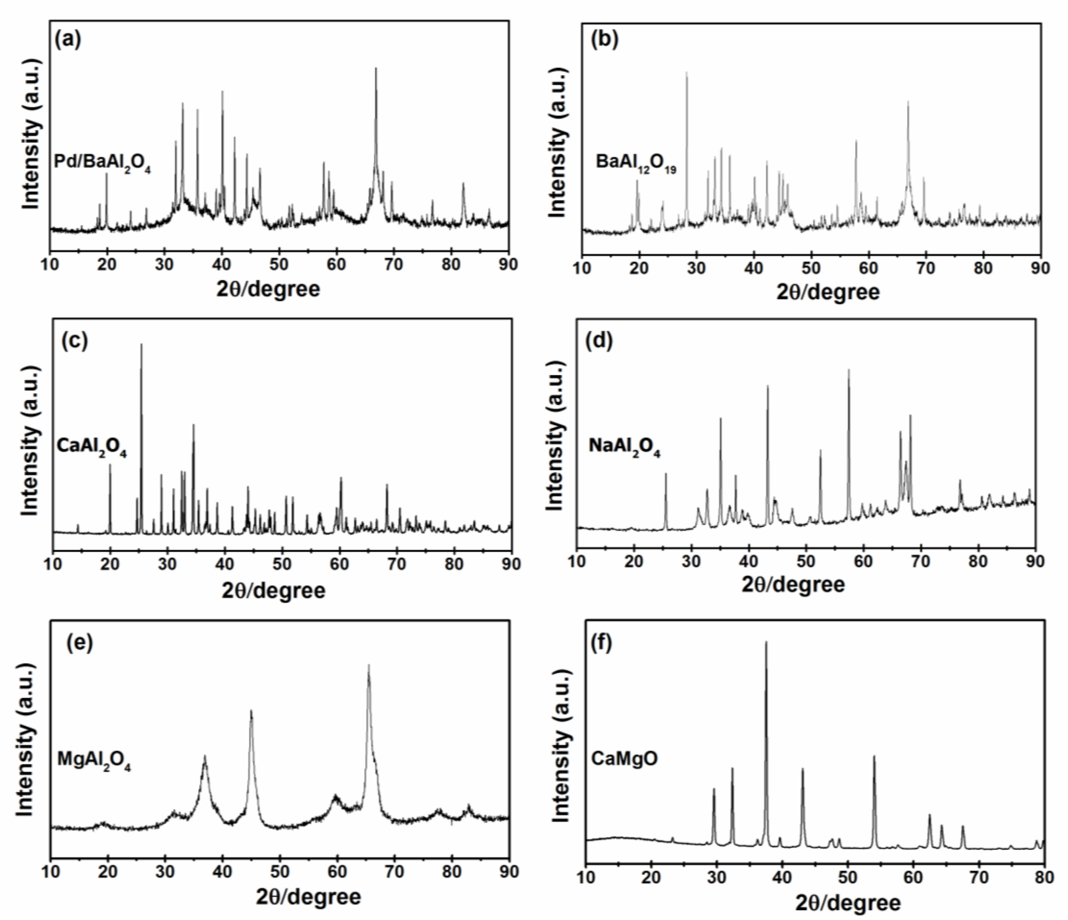


**Fig. S1.** Powder X-ray diffraction patterns of (a) 5 wt% Pd/$BaAl_{12}O_{19}$, (b) $BaAl_{12}O_{19}$, (c) $CaAl_2O_4$, (d) $NaAl_2O_4$, e) $MgAl_2O_4$, (f) CaMgO catalysts.

## 2.2. BET surface area and acidity/basicity of the catalysts

The BET surface area and acid base density of the as-synthesized catalysts are shown in table S1 and table S2. The texture of the catalysts was dependent on the base metal present in the structure and the higher surface area and pore volume resulted in a significant decrease in the crystallite size area. Among variety of heterogeneous catalysts, $MgAl_2O_4$ catalyst exhibited high (105.4 $m^2$ $g^{-1}$). It was observed that the addition of palladium in the catalysts significantly reduce the surface area of the catalysts (Table S1). This could be attributed to the blocking of the narrow pores of the structure with the active metal component making it inaccessible to nitrogen molecules.

**Table S1**. BET surface area of Pd based heterogeneous catalysts.

| Entry | Catalyst | S [$m^2\ g^{-1}$] |
|---|---|---|
| 1 | Pd/C | 425 [a] |
| 2 | Ru/C | 3.0 [a] |
| 3 | Pt/C | 100 [a] |
| 4 | Pd/$Al_2O_3$ | 148 [a] |
| 5 | Pd/$ZrO_2$ | 49 [a] |
| 6 | Pd/$SiO_2$ | 253 [a] |
| 7 | Pd/$BaSO_4$ | 5.0 [a] |
| 8 | Pd/$MgAl_2O_4$ | 89.7 [b] |
| 9 | Pd/$CaAl_2O_4$ | 5.2 [b] |
| 10 | Pd/$BaAl_{12}O_{19}$ | 52.4 [b] |

[a] Commercial catalysts; characterised in literature.[3–4] [b] Self-prepared and characterized catalysts.

It was observed that the basic character of the catalysts is strongly pronounced by the presence of alkaline metal (Table S2). In general, the basic sites are generated from the ionic character of metal to unsaturated cation bond. Depending on the strength of the ionic character, these basic sites can be discerned as Lewis (weak) basic sites and Brønsted (strong) basic sites. In the as-synthesized catalysts, CaMgO catalyst exhibited high basicity compare to the other hexa-aluminate catalysts.

**Table S2**. BET surface area and acidity/basicity of the heterogeneous catalysts.

| Entry | Catalyst | S [$m^2\ g^{-1}$] | Total acidity [mmol $g^{-1}$] | Total basicity [mmol $g^{-1}$] |
|---|---|---|---|---|
| 1 | $MgAl_2O_4$ | 105.4 [a] | - | 1.0 [a] |
| 2 | $NaAl_2O_4$ | 39.7 [a] | - | 1.2 [a] |
| 3 | $CaAl_2O_4$ | 8.2 [a] | - | 1.1 [a] |
| 4 | $BaAl_{12}O_{19}$ | 94.8 [a] | - | 0.7 [a] |
| 5 | CaMgO | 15.5 [b] | - | 3.0 [a] |
| 6 | Amberlyst-15 | 42.5 [b] | 2.5 [b] | - |
| 7 | BEA-300 | 329 [b] | 0.19 [b] | - |
| 8 | HY-30 | 941 [b] | 0.29 [b] | - |
| 9 | HY-80 | 549 [b] | 0.69 [b] | - |
| 10 | ZSM5-30 | 390 [b] | 1.12 [b] | - |

[a] Self-prepared and characterized catalysts. [b] Commercial catalysts; characterised in literature.[5-6]

## 2.3. Morphology of the catalysts

The high resolution TEM images of $NaAl_2O_4$ and $CaAl_2O_4$ catalyst showed big and coarse crystallites and agglomerates with sharp needle or worm like morphology (Fig. S2a-b). TEM image of $BaAl_{12}O_{19}$ catalyst exhibited two distinctive morphologies, one with big crystallites and the other one with small agglomerates. Big crystallites seem to grow in the form and shape of platelets and the small agglomerates show features in the form of needle or 3D worm-like (Fig. S2c). The morphology of $CaAl_2O_4$ catalyst consists mainly of porous platelets of different nanometric sizes. In the selective area electron diffraction patterns (SAED) of $NaAl_2O_4$, $CaAl_2O_4$ and $BaAl_{12}O_{19}$ catalysts clear diffraction spots are observed characteristic of crystalline order. The amorphous structure of $MgAl_2O_4$ catalyst was confirmed by SAED pattern, matches well with the XRD data (Fig. S2d).

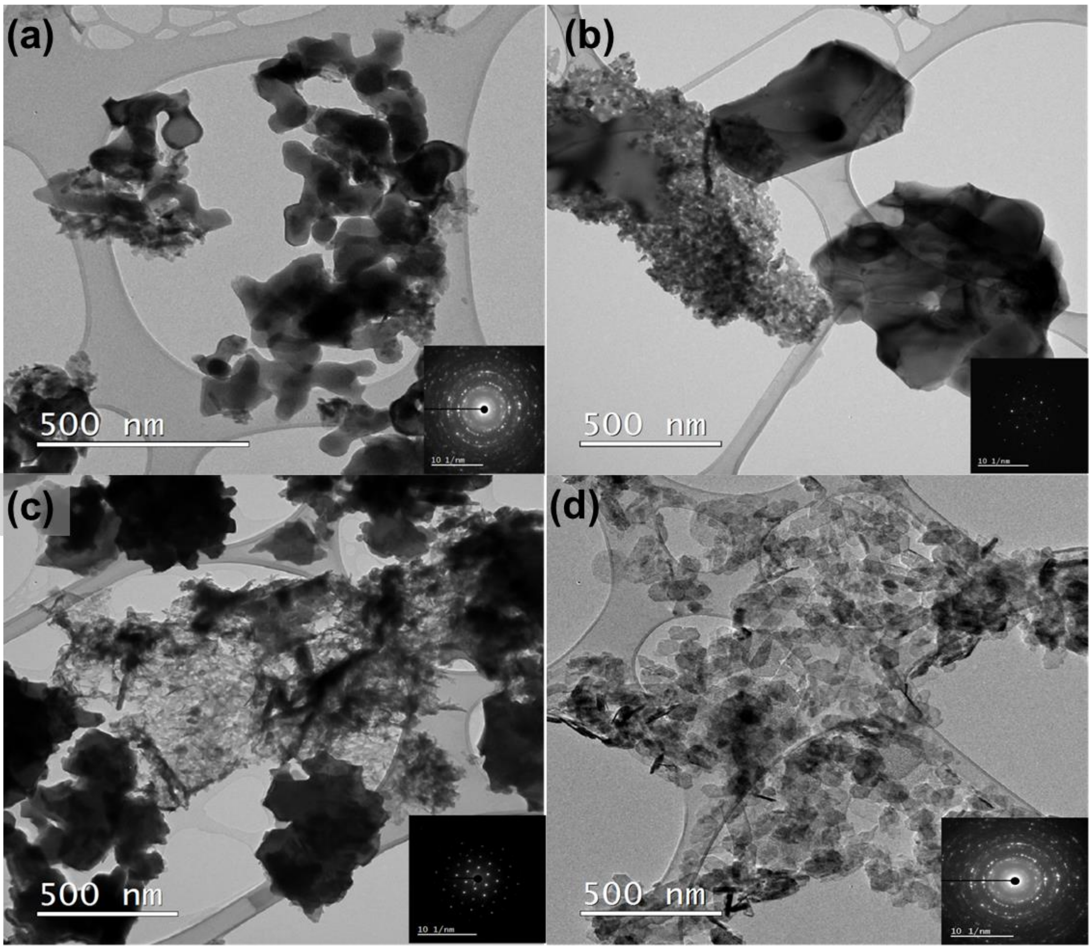


**Fig. S2** Transmission electron micrographs and electron diffraction pattern (inset) of (a) $NaAl_2O_4$ (b) $CaAl_2O_4$ (c) $BaAl_{12}O_{19}$ and (d) $MgAl_2O_4$ catalysts.

**Table S3** Molecular information and physical properties of the Copolymers. $M_n$, $M_w$, and PDI were determined by GPC.

| **Copolymer** | **$M_n$ (g mol$^{-1}$)** | **$M_w$ (g mol$^{-1}$)** | **PDI** | **$T_g$ (°C)** | **$T_{10}$ (°C)** | **$T_d$ (°C)** |
|---|---|---|---|---|---|---|
| Bio-MAA based copolymer | 53 593 | 36700 | 1.45 | 23 | 260 | 398 |
| Petroleum derived MAA based copolymer | 54 399 | 35100 | 1.54 | 25 | 270 | 410 |

$T_{10}$ and $T_d$ are the temperatures for 10 % weight loss and the temperature for decomposition, respectively, according to the TGA data.

**Table S4** Final 'technical-data-sheet' properties of synthesized copolymers.

| **Parameter** | **Unit** | **Required value** | **Petroleum derived MAA based copolymer** | **Bio-MAA based copolymer** |
|---|---|---|---|---|
| Solid content | wt% | 59.0-61.0 | 60.10 | 59.90 |
| Viscosity @ 20 °C, 100 s$^{-1}$ | Pas | 4.50-6.50 | 5.95 | 5.18 |
| Acid Number | mgKOH/g $_{100\%}$ | 19.0-23.0 | 22.0 | 21.7 |
| Color index | Hazen | < 100 | 35 | 45 |

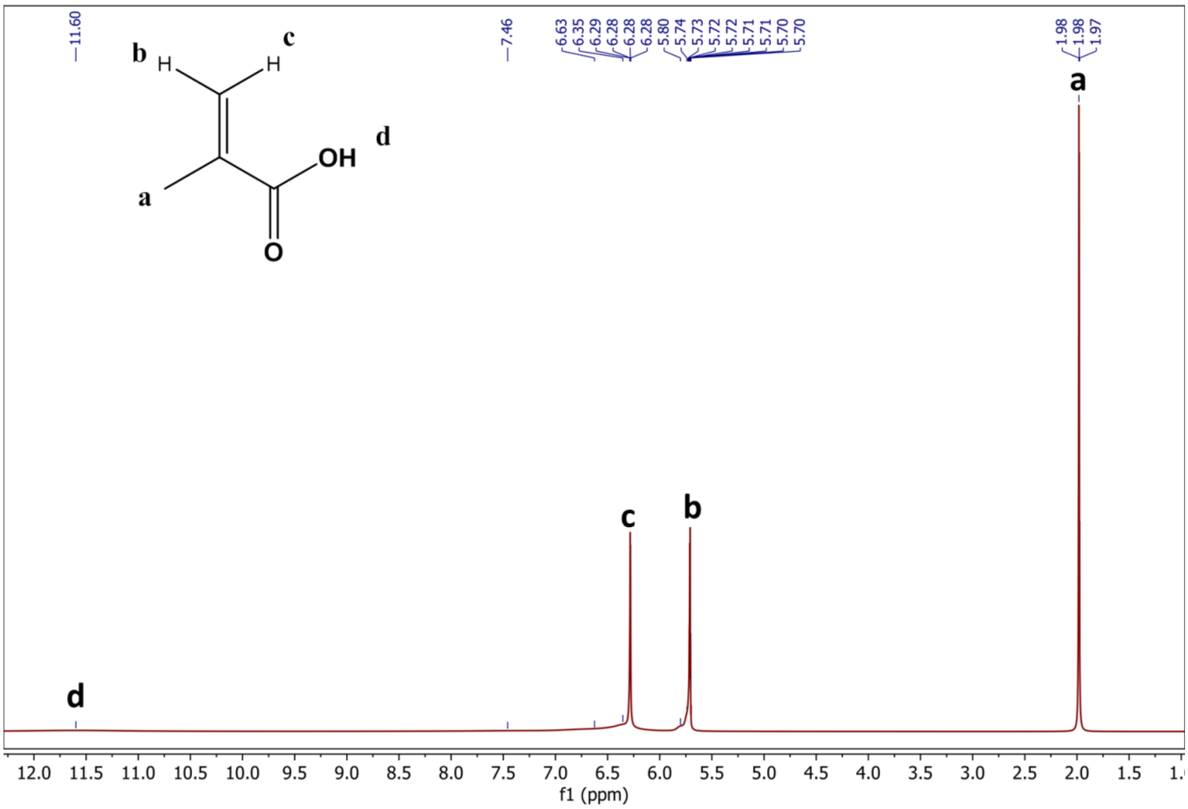


**Fig. S3** $^{1}H$-NMR of methacrylic acid after purification.

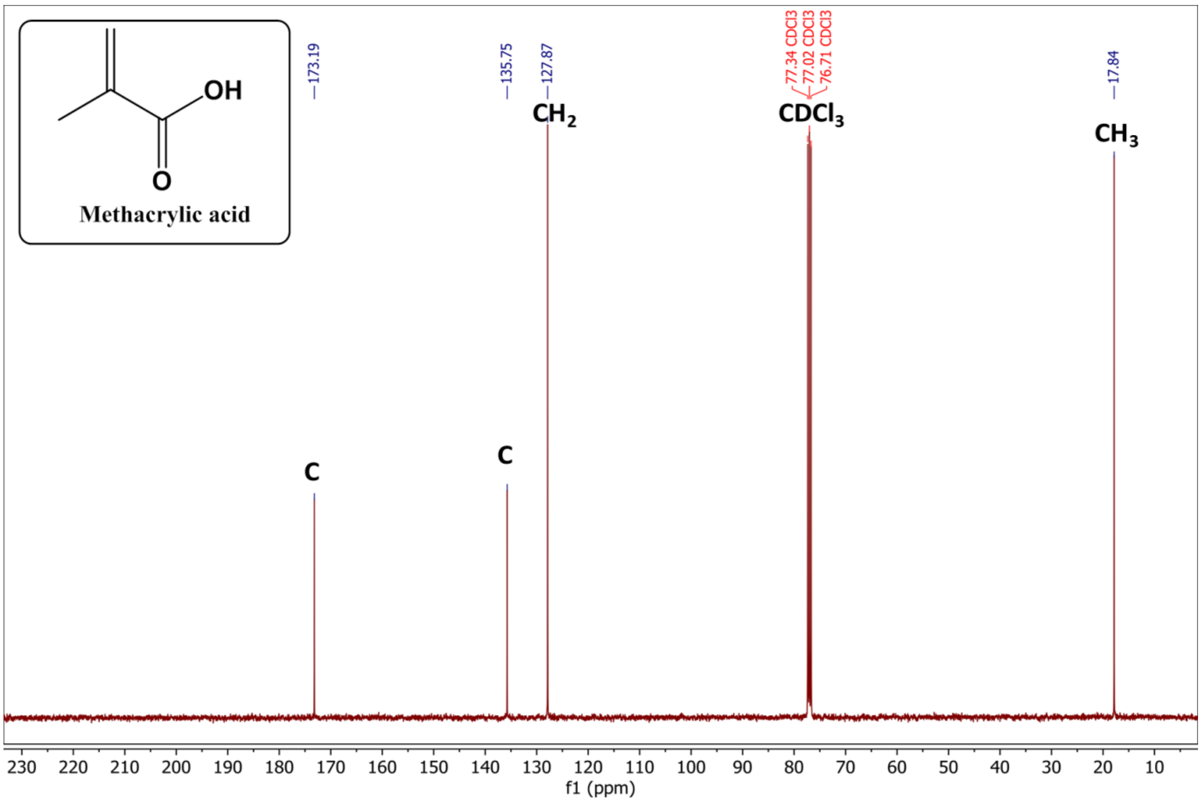


**Fig. S4** $^{13}C$-NMR of methacrylic acid after purification.

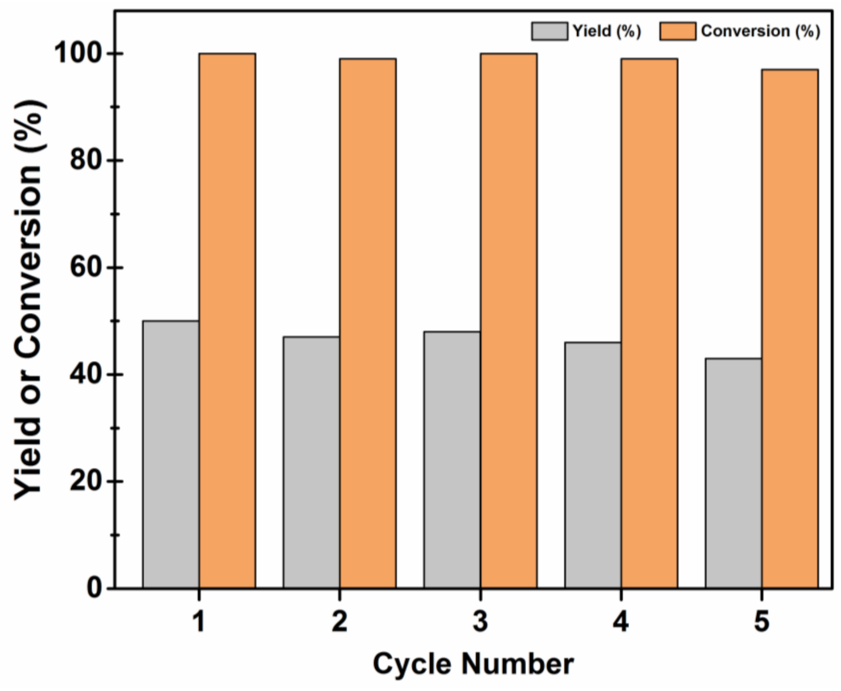


**Fig.S5** Recyclability of the $BaAl_{12}O_{19}$ catalyst. Reaction conditions: Itaconic acid (2 g), water (150 mL), catalyst (1 g), initial pressure (20 bar).

## References


1. Gao, J.; Jia, C.; Li, J.; Gu, F.; Xu, G.; Zhong, Z.; Su, F., Nickel catalysts supported on barium hexaaluminate for enhanced CO methanation. *Industrial & Engineering Chemistry Research* **2012,** *51* (31), 10345-10353.
2. (a) Debsikdar, J. C., Synthesis and characterization of gel-derived barium hexa-aluminate. *J. Mater. Sci.* **1989,** *24* (10), 3565-3572; (b) Laachachi, A.; Ferriol, M.; Cochez, M.; Lopez Cuesta, J. M.; Ruch, D., A comparison of the role of boehmite (AlOOH) and alumina (Al2O3) in the thermal stability and flammability of poly(methyl methacrylate). *Polymer Degradation and Stability* **2009,** *94* (9), 1373-1378.
3. De Schouwer, F.; Claes, L.; Claes, N.; Bals, S.; Degrève, J.; De Vos, D. E., Pd-catalyzed decarboxylation of glutamic acid and pyroglutamic acid to bio-based 2-pyrrolidone. *Green Chemistry* **2015,** *17* (4), 2263-2270.
4. Verduyckt, J.; De Vos, D. E., Highly selective one-step dehydration, decarboxylation and hydrogenation of citric acid to methylsuccinic acid. *Chemical science* **2017,** *8* (4), 2616-2620.
5. (a) Harikrishna, Y.; Kumar, V. P.; Ramu, K.; Chary, K. V.; Rao, V. V., Catalytic functionalities of Pd catalysts supported on spinel MgAl 2 O 4 for coupling of

ethylbenzene dehydrogenation with nitrobenzene hydrogenation. *Applied Petrochemical Research* **2015,** *5* (1), 71-80; (b) Dutta, S.; Bohre, A.; Zheng, W.; Jenness, G. R.; Núñez, M.; Saha, B.; Vlachos, D. G., Solventless C–C Coupling of Low Carbon Furanics to High Carbon Fuel Precursors Using an Improved Graphene Oxide Carbocatalyst. *ACS Catalysis* **2017,** *7* (6), 3905-3915.

**6.** (a) Lee, H. V.; Juan, J. C.; Abdullah, N. F. B.; Taufiq-Yap, Y. H., Heterogeneous base catalysts for edible palm and non-edible Jatropha-based biodiesel production. *Chemistry Central Journal* **2014,** *8* (1), 30; (b) Engtrakul, C.; Mukarakate, C.; Starace, A. K.; Magrini, K. A.; Rogers, A. K.; Yung, M. M., Effect of ZSM-5 acidity on aromatic product selectivity during upgrading of pine pyrolysis vapors. *Catal. Today* **2016,** *269*, 175-181; (c) Teo, S. H.; Taufiq-Yap, Y.; Ng, F., Alumina supported/unsupported mixed oxides of Ca and Mg as heterogeneous catalysts for transesterification of Nannochloropsis sp. microalga’s oil. *Energy Convers. Manage.* **2014,** *88*, 1193-1199.